Construction and Building Materials 458 (2025) 139143

Contents lists available at ScienceDirect

Construction and Building Materials

journal homepage: www.elsevier.com/locate/conbuildmat

Functionalized biochar for carbon neutral/negative cementitious composites with superior performances

Nishad Ahmed, Adhora Tahsin, Farzana Mustari Nishat, Warda Ashraf *

Department of Civil Engineering, University of Texas at Arlington, USA

ARTICLE INFO

Keywords:
Biochar
Carbon-negative cement
Functionalized biochar
Polydopamine
Polyacrylic acid
Life cycle assessment

ABSTRACT

This article presents a novel method to produce carbon-neutral and carbon-negative cementitious composites using different types of functionalized biochar. Wood-based biochar was chemo-mechanically altered using two organic additives – polydopamine (PDA) and polyacrylic acid (PAA). This functionalized biochar was added at a dosage of up to 30 % by weight of the binder. The mortar samples' compressive strength and microstructural properties were monitored after 7, 28, and 56 days of two different curing conditions, i.e., sealed curing and carbonation curing. This investigation reveals that the addition of functionalized biochar improves the workability and hydration kinetics of cementitious composites compared to those containing raw biochar. Without any modification, the addition of such high dosages of biochar results in a maximum of 8 MPa compressive strength after 56 days of curing. With the developed modification, the same biochar dosage resulted in a maximum 54 MPa compressive strength after the same curing duration. The 56-day compressive strength of the mortar samples containing functionalized biochar was increased up to 22 % for sealed curing and 24 % for carbonation curing compared to the control batch (without biochar). The superior properties of functionalized biochar were attributed to PDA and PAA which enhanced the performance of composites by strengthening the adhesion between the binder and functionalized biochar particles. The life cycle assessment (LCA) showed that nearly all biochar batches subjected to carbonation curing exhibited negative carbon footprints, with GWP reductions ranging from 90 % to 170 % compared to the control batch.

1. Introduction

CO_2 emissions increased by 53 % worldwide from 1990 to 2020, adversely impacting the climate and the ecosystem [1]. Currently, many countries (e.g., the European Union and USA) are trying to achieve carbon neutrality by 2050 [2,3]. More than 1000 cities and educational institutes, over 9000 companies, and around 600 financial institutes have joined 'Race to Zero' to take immediate action to halve global emissions by 2030 [4]. To achieve this goal, the carbon footprint of the most widely used infrastructure material - concrete, also needs to be drastically reduced. Concrete is the second most consumed material in the world after water [5]. Ordinary Portland Cement (OPC) - the key ingredient of concrete is produced at a rate of 4 billion metric tons per year [6]. The cement and concrete industry is also responsible for nearly 8 % of global CO_2 emissions [7]. This industry is considered one of the 'hard to decarbonize' sectors and requires new innovations to achieve the net zero goal. While supplementary cementitious materials (SCM) such as fly ash, slag, and silica fume can be good alternatives to OPC for reducing the CO_2 footprint of concrete, producing carbon-neutral/negative cementitious materials using SCM is challenging due to their limited carbon sequestration capacity.

To achieve carbon neutrality of concrete, a significant amount of carbon sequestration is required, which can be achieved by using biochar [5,8–11]. Biochar is produced from the pyrolysis of biomass. Biomass, like forest residue, sequesters CO_2 from the atmosphere as its growing mechanism, which can be again released into the atmosphere while getting decomposed by microorganisms [12]. Onsite incineration of this residue can adversely affect soil productivity by modifying microbial populations, eradicating seeds, and creating bare soil [13]. Therefore, pyrolysis, which is a thermomechanical process carried out in an oxygen-limited environment, was introduced as a feasible option for converting the organic carbon in biomass into solid (biochar), liquid (bio-oil), and gaseous (syngas) carbonaceous products [14,15]. Typically, the net energy production from the pyrolysis of wood waste for biochar generation is 38 % less than incineration [16]. Of the two pyrolysis processes, slow pyrolysis yields higher amounts of biochar,

* Corresponding author.
E-mail address: warda.ashraf@uta.edu (W. Ashraf).

https://doi.org/10.1016/j.conbuildmat.2024.139143
Received 23 June 2024; Received in revised form 29 September 2024; Accepted 8 November 2024
Available online 22 December 2024

whereas fast pyrolysis enhances bio-oil production [17,18].

By carefully controlling factors such as feedstock type, moisture content, and ash content, the addition of biochar offers a pathway to achieve a lower carbon footprint compared to other bio-based building materials like hemp fiber [19,20]. According to Zampori et al., the global warming potential (GWP) of hemp fiber, with a yield of 15 %, is −1.73 kg CO_2 eq/kg [19]. Similarly, biochar produced from wood residue with a comparable yield efficiency of 16 % has a GWP ranging from −1.6 to −2.1 kg CO_2 eq/kg [19,20]. Although the stability of biochar is strongly influenced by the feedstock type and the conditions of pyrolysis, stable polycyclic aromatic carbon (SPAC) formation can be achieved through high-temperature pyrolysis[21] This SPAC remains stable in biochar over a centennial timescale, thus ensuring carbon sequestration in biochar composites for hundreds to thousands of years [21,22]. Such long-term carbon sequestration is not achievable using other bio-based or wood-based composites, as their decay liberates carbon in the form of carbon dioxide or methane in the atmosphere [23].

In the past few years, a great volume of work has been done on the usage of biochar in cement-based composites, primarily due to their internal curing capacity [24–28]. However, the challenge is the negative effect of biochar on the mechanical performance of the composites. Most of the past studies used a small dosage (up to 10 % of the binder) of biochar and observed no or negligible benefits in enhancing the compressive strength of the composites [8,29–31]. Such biochar dosages are too low to offset the CO_2 emitted during cement production and not adequate to achieve carbon neutrality. On the other hand, when a high dosage of biochar (up to 30 % by weight of the binder) is used, a drastic reduction in the strength of cementitious composites was observed. For example, Chen et al. replaced the fine aggregate with up to 30 % biochar to produce carbon-neutral concrete with 28 days of compressive strength of around 13 MPa [5]. Such a range of compressive strength is typically considered too low for structural concrete applications. Li and Shi [9] also developed a carbon-negative concrete using 30 wt% CO_2-weather biochar and 70 wt% Portland limestone cement with a 28-day compressive strength of 27.6 MPa. In their study, the control batch (without biochar) showed a compressive strength of around 50 MPa at 28 days, indicating a nearly 45 % reduction in strength due to the addition of biochar. Though the use of biochar is one of the most promising pathways to produce carbon-neutral concrete, the corresponding reduction in strength makes it less convincing for the end users, causing a blockade toward net zero movement. Therefore, identifying potential pathways to utilize biochar for carbon sequestration, which also enhances the performance of the composite compared to the traditional composites (concrete without biochar), is a crucial research need.

Aiming to improve the overall performance of carbon-neutral cementitious composites using higher biochar dosage, this paper evaluated novel chemo-mechanical modifications of biochar using two organic additives. These additives are polydopamine (PDA) and polyacrylic acid (PAA). The usage of polydopamine to improve the binding in synthetic materials is gaining popularity because of its high adhesive properties [32,33]. Mussels can release high adhesive proteins composed of L-3,4-dihydroxyphenylalanine (DOPA) and lysine, by which they can attach to various underwater substrates. Dopamine also contains the same catechol and amine functional group, making it an excellent adhesive to other inorganic and organic materials due to its ability to self-polymerize to form PDA film [34]. Khan et al. utilized PDA to investigate the CO_2 curing effect on cementitious composites [35], whereas Fang et al. used PDA with very fine aggregate to improve its adhesion with binder particles [36]. Similarly, Chen et al. also used PDA with crumb rubber to enhance the performance of rubberized cementitious materials [37]. On the other hand, polyacrylic acid (PAA) is one of the most popular polymers used in polymer-modified cement-based materials. The carboxyl group of PAA could combine with Ca^{2+} ions present in the pore solution and the surface of the cement particles, affecting cementitious materials' dispersion and rheological properties [38]. In this study, PAA was selected due to its ability to enhance workability and improve the performance of CO_2-cured composites.

This paper aims to investigate the effect of PDA and PAA on cementitious material containing higher dosages of biochar with two different curing conditions: (I) sealed curing and (II) CO_2 curing. The specific goals of this research work were as follows: (I) to produce carbon-negative cementitious composites with superior mechanical performance, (II) to investigate the effects of functionalized biochar on the workability and the hydration of cementitious materials, (III) to investigate the effects of different curing conditions (sealed curing and CO_2 curing) and functionalized biochar on the macroscale (compressive strength) and microscale performances of carbon neutral cementitious composites.

2. Materials and methods

2.1. Raw materials

The raw materials used in this study were ordinary Portland cement (OPC), slag cement, biochar, and river sand. The chemical composition of OPC and slag cement was measured by X-ray fluorescence (XRF), shown in Table 1. OPC and slag were mixed in a 1:1 ratio to produce a blended binder. Slag was used to achieve a lower carbon footprint of the blended binder.

The materials' particle size distribution (PSD) was obtained using a laser particle size analyzer (Shown in Fig. 1). Biochar was supplied by a commercial supplier. They used a slow pyrolysis kiln to produce biochar from wood materials by keeping it at 1250°F for up to 10 hours in a vacuum. The TGA and derivative of thermogravimetry (DTG) graph of biochar is shown in Fig. 2. Table 2 represents the characteristics of raw biochar as obtained from the supplier. Different dosages of dopamine hydrochloride ($C_8H_{11}NO_2$-HCl, 99 %) and Polyacrylic acid $(C_3H_4O_2)_n$ (molecular weight-2000) were used to modify the biochar.

2.2. Sample preparation

2.2.1. Functionalized biochar preparation

Inspired by a prior study of producing super-hydrophobic additive from biochar [39], a similar chemo-mechanical modification approach was followed, but with different target functionality. Three different functionalized biochar batches were produced in this study: Bio_Grn, Bio_PDA, and Bio_PAA. The production of Bio_Grn only involved a mechanical process as it was produced by grinding raw biochar in a ball mill for 2 hours. For Bio_PDA, the biochar was ground for one hour, then DOPA was added at a dosage of 2 % by wt. of biochar, and again ground for one hour. The same procedure was followed to produce Bio_PAA, where PAA was added instead of PDA. The rotation speed of the ball mill was 2520 rpm for uniform blending. Four nylon jars with 8 pieces of zirconia balls of 4 different sizes per jar were used to grind the biochar. The particle size distributions of these functionalized biochar batches compared to that of the binder are shown in Fig. 1. The schematic showing the sample preparation and test setup is depicted in Fig. 3.

2.2.2. Test sample preparation

The mixture proportions, as shown in Table 3, were designed to obtain carbon-negative and carbon-neutral batches using different biochar dosages. Paste samples were prepared to observe the cement hydration and microstructural properties. Mortar samples were prepared

Table 1
Oxide contents of OPC and slag cement used in this study.

Cement types\ Oxide contents	CaO	SiO_2	Fe_2O_3	Al_2O_3	SO_3	MgO	K_2O
OPC	65.3	21.2	3.10	3.87	4.28	0.816	0.679
Slag	36.4	29.6	0.372	15.6	5.19	9.69	0.305

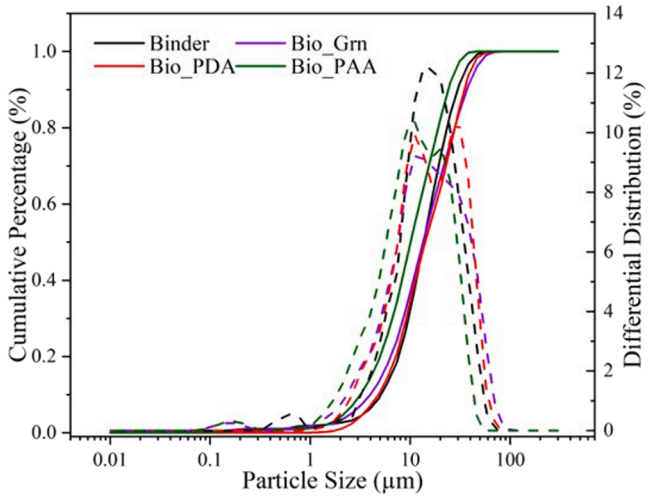

Fig. 1. Particle size distribution of different batches.

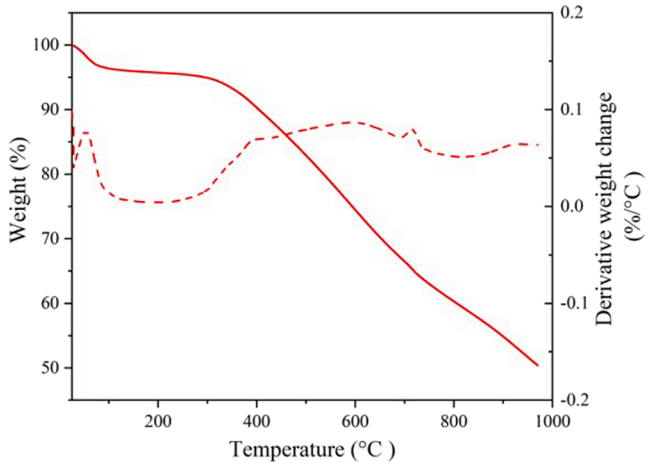

Fig. 2. Thermogravimetric analysis (TGA) plots of biochar.

Table 2
Characteristics of raw biochar.

Parameters	Units
Carbon	87.4 (% of total dry mass)
Hydrogen	3.5 (% of total dry mass)
Nitrogen	0.53 (% of total dry mass)
Total Ash	2.1 (% of total dry mass)
Surface area	308 m^2/g (dry)
Bulk density	8.8 lb/cu ft

to evaluate the mechanical properties and carbon footprint. The functionalized biochar was added at 23 % and 30 % by wt. of binder to obtain carbon-neutral and carbon-negative batches, respectively, which was determined by an approximate carbon sequestration capacity of 3.2 kg CO_2 eq/kg of biochar considering 87.4 % solid carbon content [30]. The water-to-binder ratio was 0.55, and the aggregate-to-binder ratio was 2.75.

For mortar sample preparation, the slag and OPC were mixed in a Hobart mixer for 2 minutes at a slow speed (140 ± 10 rpm). After that, ASTM C305 [40] was followed to prepare the mortar mix. After mixing the binder, water, and sand according to ASTM C305, biochar was added to the mixture and then first mixed at a medium speed (285 ± 10 rpm) for 60 seconds and then at a high speed (580 ± 10 rpm) for 30 seconds.

To prepare paste samples, the biochar was mixed with the binder for one minute (dry mix) to ensure uniform distribution of all materials. Then, water was added to the dry mixture and mixed at 350 rpm for 1.5 minutes. These paste samples were used to determine the microstructural properties using thermogravimetric analysis (TGA), X-ray diffraction (XRD), and backscattered electron (BSE) after both carbonation and sealed curing.

Two sets of mortar and paste samples were prepared. All the samples were demolded after 24 hours of casting. One set was subjected to sealed curing, and another set was subjected to accelerated carbonation curing. For the accelerated carbonation curing, samples were kept in the carbonation chamber at 20 % CO_2 concentration, 65 % relative humidity, and 25°C temperature until testing.

2.3. Experimental methods

2.3.1. Zeta potential of functionalized biochar

The zeta potential of the blended binder and different functionalized biochar was measured using the nanopartica SZ-100 from Horiba Scientific. The suspensions were prepared using deionized water and contained 0.003 % samples. Sonics Vibra Cell VCX 750 Ultrasonic Liquid Processor was used to disperse the suspension for 80 seconds before measuring the zeta potential.

2.3.2. Workability measurements

Flow table test was performed according to ASTM C1437 [41] to determine the workability of mortar mixtures containing different dosages of functionalized biochar.

2.3.3. Strength measurements

The compressive strengths of 50 mm by 50 mm mortar cubes were measured using a Universal Testing Machine with a load rate of 200 lb/s–400 lb/s according to ASTM C109 [42]. The compressive strength of mortar samples was measured after 7 days, 28 days, and 56 days of carbonation and sealed curing.

2.3.4. Effects on cement hydration rate and product

An isothermal calorimeter (TAM AIR, TA Instrument) with admixture ampoules was used to measure the total heat release and heat flow from the paste samples up to 7 days at an ambient temperature of 25°C. First, dry mixtures of OPC, slag, and biochar were prepared for different batches according to Table 3. Then, approximately 5 g of the dry sample was put in a glass ampoule and placed in the isothermal calorimeter chambers. After putting the samples inside the calorimeter chambers, it took around 45 minutes to stabilize the heat flow signals. After the signals were stabilized, distilled water was added to the dry mix using syringes. The measurement of the heat of reaction started immediately after adding water and continued for up to 7 days. The isothermal calorimeter test was conducted twice to ensure the reliability and repeatability of the results.

2.3.5. Density

The fresh density was measured for all the batches by using a cylindrical plastic container. First, the weight of the empty container was measured, and then it was filled with water to determine its volume. Finally, the container was filled with mortar samples in three layers of approximately equal volumes. After filling each layer, it was rodded 25 times with a temping rod according to ASTM C138 [43]. The side of the container was also tapped gently to release any trapped air bubbles inside the mortar sample. Finally, the weight of the samples was taken to determine the density. The fresh density of the mortar was calculated by dividing the mortar weight by the volume of the container.

2.3.6. Thermogravimetric analysis (TGA)

Paste samples were used for thermogravimetric analysis (TGA). Isopropanol was used to stop hydration after 7 days, 28 days, and 56 days of curing following the solvent exchange method. The paste sam-

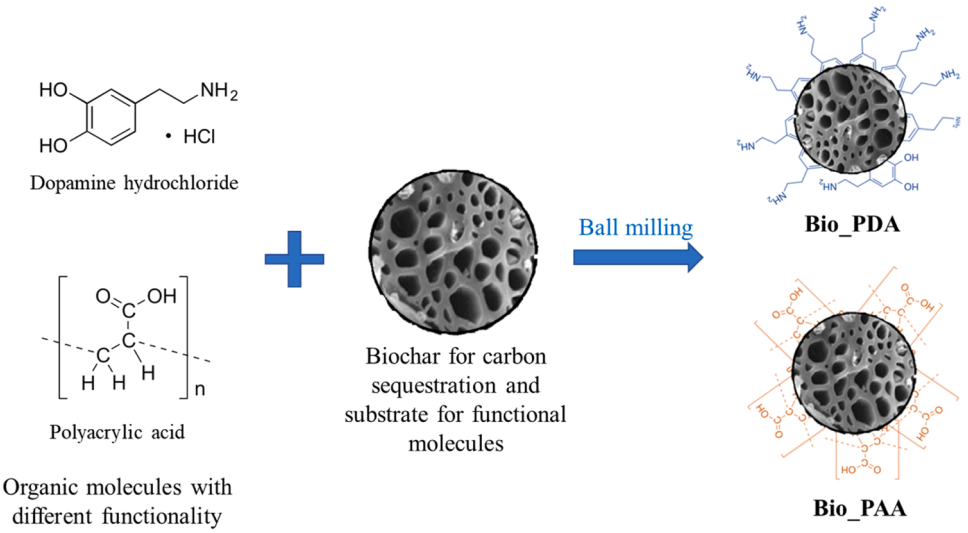

Fig. 3. Schematic showing the sample preparation and test setup.

Table 3
Mix design (with respect to 100 gm of binder).

Sample ID	OPC (g)	Slag cement (g)	Aggregate (g)	Water (g)	Biochar (g)	PDA (g)	PAA (g)
Control	50	50	275	55	0	0	0
*Bio_Control_23 %	50	50	275	55	23	0	0
*Bio_Control_30 %	50	50	275	55	30	0	0
Bio_Grn_23 %	50	50	275	55	23	0	0
Bio_Grn_30 %	50	50	275	55	30	0	0
Bio_PDA_23 %	50	50	275	55	23	0.46	0
Bio_PDA_30 %	50	50	275	55	30	0.6	0
Bio_PAA_23 %	50	50	275	55	23	0	0.46
Bio_PAA_30 %	50	50	275	55	30	0	0.6

OPC: Ordinary Portland Cement, PDA: Polydopamine, PAA: Polyacrylic Acid.
* Raw Biochar

ples were then dried in a desiccator for 3 days to avoid atmospheric carbonation. The thermal analysis was performed using a commercially available instrument (TA instrument, TGA 550). Approximately 35–40 mg of ground paste sample was prepared for TGA measurement using a mortar and pestle. The powdered samples were loaded into a platinum pan and kept under isothermal conditions at around 25°C for 3 minutes, and then the temperature was raised continuously at a rate of 15°C per minute up to 980°C. Nitrogen was used as a purging gas during the test to maintain an inert environment. Mass losses in the 550–900°C range were used to calculate the carbonated samples' calcium carbonate ($CaCO_3$) mass fraction. The calculation of carbonate content is done according to the reference [44]. The $CaCO_3$ calculation was adjusted due to the mass loss of biochar in the same temperature range. The TGA and derivative of thermogravimetry (DTG) graph of biochar is shown in Fig. 2. Eq. 1 is used to determine the $CaCO_3$ content without biochar adjustment, which means biochar decomposition was not considered in this calculation. However, Eq. 2 is used to determine the $CaCO_3$ content with biochar adjustment. In Eq. 2, the weight loss of biochar in 550–900°C is determined by using Eq. 3. In Eq. 3, the weight loss of biochar obtained from Fig. 2 is multiplied by the amount of biochar in 100 g of paste sample. This multiplication provided the total weight loss of biochar in 550–900°C temperature range. The chemically bound water was calculated by subtracting the mass losses due to the decomposition of $CaCO_3$ (550–900°C) and free water (mass loss below 100°C) from the total mass loss up to 980°C [45].

$$CaCO_{3,measured}\ (\%) = Weight\ loss_{CaCO_3} \times \frac{mass_{CaCO_3}}{mass_{CO_2}} \quad (1)$$

$$CaCO_{3,measured}\ (\%) = Weight\ loss_{CaCO_3} \times \frac{mass_{CaCO_3}}{mass_{CO_2}} - Weight\ loss_{Biochar} \quad (2)$$

$$Weight\ loss_{Biochar}(\%) = Weight\ loss_{Biochar(from\ TGA\ graph\ of\ biochar)} \times Biochar\ weight\ \ in\ 100g\ of\ paste\ sample. \quad (3)$$

2.3.7. Scanning electron microscope (SEM)

The microstructure of biochar batches was analyzed with a high-resolution scanning electron microscope (HITACHI 3000 N SEM). The samples were embedded in epoxy for the SEM-EDS analysis. The aspect ratio of the needle-shaped biochar particles was measured using image analysis.

2.3.8. X-ray diffraction (XRD)

X-ray diffraction (XRD) analysis of paste samples was conducted on a Bruker D-8 spectrometer using Cu Kα radiation (40 kV, 40 mA). The diffraction patterns were obtained over 5°–60° (2θ) ranges with a step size of 0.03 per second.

2.3.9. Life cycle assessment (LCA)

2.3.9.1. Goal and scope definition. The global warming potential (GWP) for most of the raw materials was acquired from the Ecoinvent 3 dataset, assessed by TRACI (The Tool for the Reduction and Assessment of Chemical and Other Environmental Impacts), and the analysis was conducted using SimaPro 9.0.0.38. However, the environmental impact of biochar production varies based on factors such as feedstock types, biomass collection methods, diverse production locations, and various power sources utilized in the production process [46]; furthermore, the physiochemical properties of biochar, specifically carbon content, fluctuate depending on feedstock type and pyrolysis temperature [47]. Consequently, the GWP data for biochar was compiled from various sources and employed to evaluate its impact on the variability of the ultimate carbon footprint associated with mortar. Moreover, a set of the samples was carbonation-cured to observe its effect on the mechanical and microstructural properties of mortar, which resulted in additional CO_2 sequestration in the form of calcium carbonates. This CO_2 content was determined from TGA analysis by calculating the weight reduction of paste samples within the temperature range 550 - 980°C.

2.3.9.2. Data inventory. The source of GWP for biochar is discussed in the Results section. Data on GWP for the remaining raw materials were gathered from the Ecoinvent 3 dataset. The selected material categories from this database, along with their corresponding GWP values, are presented in Table 4. The production of OPC results in the emission of approximately 1 kg of CO_2 per kg due to the high temperature needed for clinkerization and calcination of limestone. In contrast, slag is an industrial byproduct that undergoes a purification process involving quenching with water, dewatering, crushing, grinding, and storage in a pile. Consequently, substituting 50 % of OPC with slag leads to a reduction in the overall GWP of the binder. Polydopamine and polyacrylic acid were employed to enhance the overall performance of the biochar-based cementitious material. Based on SimaPro analysis, polyacrylic acid (PAA) demonstrated a GWP of 2.13 kg CO_2 eq/kg, while no specific data was available for polydopamine (PDA). Consequently, the GWP value for PDA was assumed to be similar to that of PAA.

3. Results and discussion

3.1. Characteristics of functionalized biochar

Fig. 4(a) shows the vapor adsorption isotherms and surface area of different functionalized biochar. Bio_PDA and Bio_PAA have higher moisture absorption capacity in 97.5 % relative humidity due to higher surface area compared to the Bio_Grn.

Table 4
Raw material categories from the Ecoinvent 3 dataset.

Material	Category	GWP (kg CO_2 eq/kg)
OPC	Cement, Portland (RoW)| market for | Cut-off, U	0.923
Slag	Ground granulated blast furnace slag {US}| production | Cut-off, U	0.0911
Sand	Sand (GLO)| market for | Cut-off, U	0.01167
Water	Water, deionized, from tap water, at the user (RoW)| market for water, deionized, from tap water, at user | Cut-off, U	0.0015
PAA	Acrylic acid {RoW}| market for acrylic acid | Cut-off, U	2.13

Fig. 4(b) shows the zeta potential measurements. The functional groups of PDA (Catechol groups and Amine groups) and PAA (carboxylic acid groups) contribute to the higher surface charge. A higher negative surface charge results in increased electrostatic repulsion between individual particles, which prevents particles from agglomeration, promoting better dispersion.

Fig. 4(c) and Fig. 4(d) represent the morphology of unground and ground biochar, respectively. The unground biochar has a highly porous structure with large macropores, which are inherited from the parent feedstock. Grinding the biochar helps to break down the porous particles into a finer size. As a result, the overall porosity got reduced after grinding the biochar [48].

3.2. Effects on early-age properties

3.2.1. Density and workability of fresh mortar mixtures

Fig. 5 represents the flow table measurements of the control and different biochar-containing mortar mixtures. The flowability test was continued for 60 minutes at intervals of 15 minutes. The initial flow diameter values of the Bio_Control 23 % and 30 % were 188.5 mm and 193.75 mm, respectively. Although the flow diameter of the Bio_Control batches is higher than other biochar batches, it was not a workable batch since they are completely disaggregated, which can be observed from Fig. 5(c). Because of this the flowability test was not continued at other time intervals for the Bio_Control batches. The drastic reduction in the workability of the mortar mixture containing Bio_Control (i.e., raw biochar) compared to the control batch is due to the high-water retention capacity of the porous raw biochar [49,50] and the angular shape of biochar that tries to restrain the movement of cement particles [51]. The structure of carbon in biochar particles has a high cation exchange capacity, indicating that it can bind to cations in solution by ion exchange. As a result, biochar can rapidly absorb part of the mixing water by hydrogen bonding during sample preparation, reducing the mix's flowability [50]. Most of the previous research used a lower biochar dosage because of the drastic reduction in flowability [29,30,49]. This further indicates that it is not possible to produce workable and carbon-negative/neutral cementitious composite using only raw biochar. As shown in this work, after adding the PDA or PAA modified biochar, the workability is significantly increased compared to Bio_Control and Bio_Grn batches. In high pH pore solution, dopamine hydrochloride spontaneously self-polymerizes by oxidation and subsequent cross-linking of the catechol structure to form polydopamine (PDA) film [37]. Formation of such PDA film on biochar reduces their water absorption and thus enhances the workability of mortar mixtures. The impact of PAA on flowability was more significant than PDA.

The fresh density of the mortar batches is shown in Fig. 6. As shown in this figure, the density of the mortar was reduced by 23.5 % and 30 % after adding 23 % and 30 % raw biochar, respectively, compared to the control batch. The reduction in density was expected due to the porous structure of raw biochar particles [29]. The density of the mortar mixtures containing functionalized biochar was increased compared to the sample containing raw biochar. The fresh densities of mortar containing 23 % Bio_Grn, Bio_PDA, and Bio_PAA were 96 %, 99.4 %, and 100.5 % of the control batch, respectively. The superior workability of the mortar mixtures containing Bio_PDA and Bio_PAA resulted in higher densities of the mortar mixtures containing these additives compared to the Bio_Grn batches at the same biochar dosage.

3.2.2. Cement hydration kinetics

The effects of various biochar batches on the binder's heat of hydration are shown in Fig. 7(a) and Fig. 7(b). From the heat flow plot, it is observed that the primary peak associated with the hydration product formation was shifted to the left due to the addition of Bio_Grn compared to the control batch indicating the hydration acceleration effect of this additive. Such an acceleration effect of Bio_Grn is attributed to the filler effect [49–52], that is, the Bio_Grn provided additional surface areas for

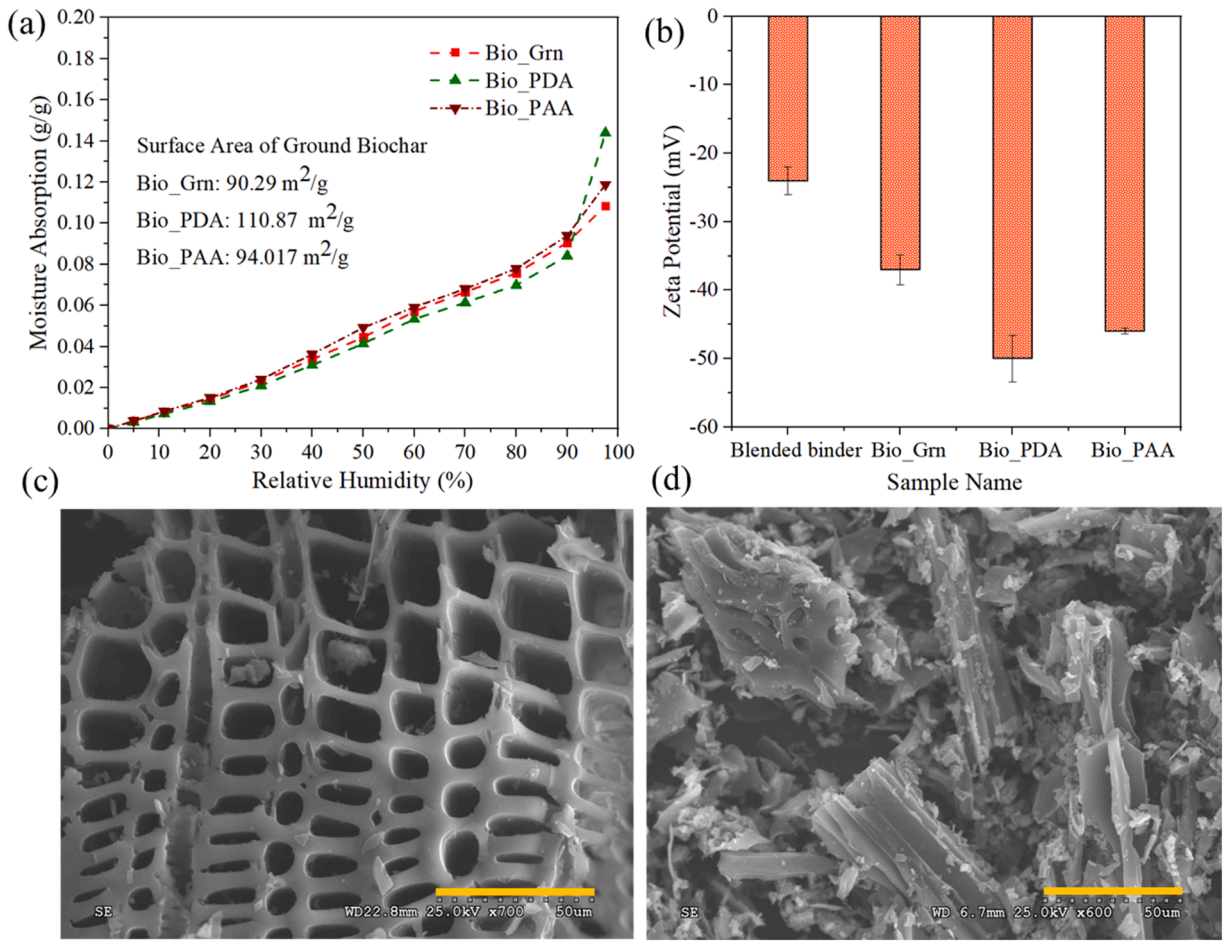

Fig. 4. (a) Moisture absorption and surface area of functionalized biochar, (b) Zeta potential of Blended binder and functionalized biochar, (c) SEM image of un-ground biochar and (d) SEM image of ground biochar. Scale bars represent 50 μm.

hydration products to nucleate, causing a faster product formation. Fig. 1 shows that grinding biochar in the ball mill produced finer particles, which was crucial for the filler effect. Similar findings were also observed in previous studies where they found increased hydration kinetics and a shorter dormant period after adding biochar as a micro filler [53–56]. The Bio_Grn containing samples also showed a higher total heat release compared to the control batch after 168 hours of hydration (Fig. 7(b)). This indicates that a higher amount of cement reacted in the Bio_Grn batch, offering a more efficient cement use compared to the control batch.

Unlike the Bio_Grn batch, the addition of Bio_PDA or Bio_PAA has negative effects on the early-age cement hydration (Fig. 7(a)). Specifically for the Bio_PDA containing samples, the primary heat flow peak was at the same location as Bio_Grn (left to the control batch), but the intensity was reduced. Therefore, the addition of Bio_PDA accelerated the cement hydration due to its surface area, but a lesser amount of cement reacted compared to the control. Such lesser hydration compared is attributed to the presence of polydopamine (PDA) in this sample. PDA has strong adhesion and affinitive interaction with Ca^{2+} because of their catechol groups [57]. The Ca^{2+} ions, available in the cement mixture, were reduced by the presence of PDA through chelating, which slowed down the formation of hydration products. Moreover, due to the binding of Ca^{2+}, PDA can get adsorbed on cement particles and reduce the available surface area for cement hydration, which further suppressed the hydration. However, as observed from Fig. 7(b), such negative effects of Bio_PDA were only apparent at an early age, and after 168 hours of hydration, the Bio_PDA containing samples showed either the same or higher heat release than the control batch.

The addition of Bio_PAA had significant negative effects on cement hydration (Fig. 7). There was no identifiable heat flow peak for these batches, and the total heat release after 168 hours was reduced by 20–30 % compared to the control batch. This negative effect on cement hydration is due to the ability of PAA to adsorb cement particles, which reduces the available surface area for cement hydration [58,59].

3.3. *Effects of functionalized biochar in sealed curing system*

3.3.1. *Role in compressive strength*

The compressive strengths of the mortars containing various biochar samples and subjected to sealed curing are shown in Fig. 8(a). The addition of raw biochar drastically reduces the compressive strength of the mortar batches compared to the control samples. Specifically, the 56 days compressive strengths of mortars containing 23 % and 30 % Bio_Control both dropped by 82 %, compared to the control batch (i.e., without biochar). After 56 days of sealed curing, these batches achieved only around 8 MPa compared to the 45 MPa compressive strength of the control batch. This drastic reduction in strength is expected due to the high void ratio of raw biochar. Therefore, the addition of raw biochar to achieve carbon neutrality of cementitious composites is impractical due to such inefficient binder use in addition to the lack of workability of the mixture (as observed in Fig. 5(c)).

Compared to the raw biochar, the compressive strengths of the mortar samples containing functionalized biochar were drastically improved. At the 23 % dosage, the addition of Bio_Grn showed 369 % higher strength compared to Bio_Control after 56 days of sealed curing.

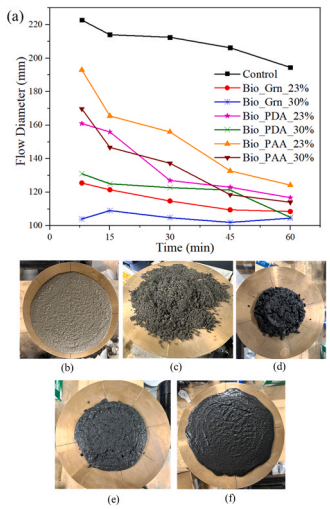

Fig. 5. Flow table test for different batches (a) flow diameter up to 60 minutes, flow table images: (b) Control (c) Bio_Control_23 % (d) Bio_Grn_23 %(e)Bio_-PDA_23 % (f) Bio_PAA_23 %.

The addition of ground biochar (i.e., Bio_Grn) instead of the raw biochar (i.e., Bio_Control) results in a denser matrix due to the reduced voids of biochar particles, and therefore resulted in a superior compressive strength. However, the strength of Bio_Grn containing samples remained less than the control batch. The 56 days compressive strength for Bio_-Grn 23 % and 30 % is 86 % and 74 %, respectively, of the control batch for sealed curing condition. The compressive strength of the mortar containing 30 % Bio_Grn was less than that of the 23 % Bio_Grn batch. Such a reduction in strength with increasing dosage of biochar is expected due to the dilution effect, i.e., reducing the amounts of cement with less reactive biochar in the unit volume of mortar.

The compressive strengths of the Bio_PDA containing mortar samples were remarkably enhanced compared to those containing raw biochar (Bio_Control) and ground biochar (Bio_Grn). The addition of 23 % Bio_PDA resulted in 28 % higher compressive strength compared to the control batch (without biochar) after 28 days of sealed curing. Such drastic enhancement of strength due to the addition of Bio_PDA was attributed to the high adhesive properties of PDA that adhered to the surface of the biochar [35] and achieved a better adhesion between the

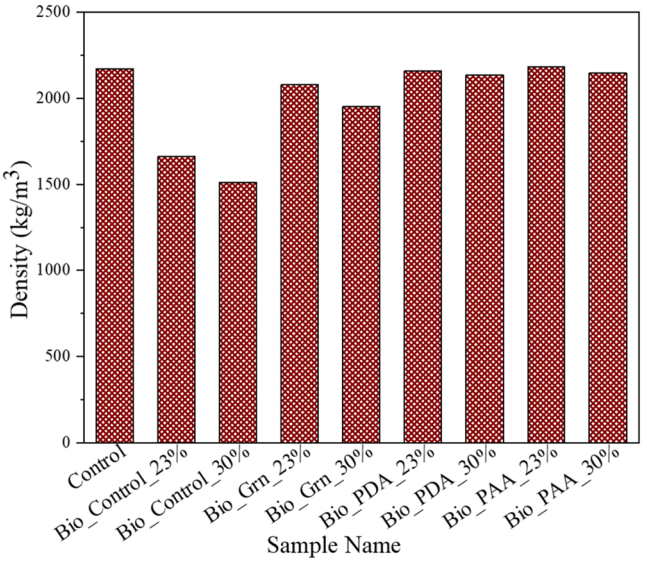

Fig. 6. Density measurement for fresh mortar mixtures containing various types of biochar.

surface of biochar and cement hydration products resulting in a densification of the cement matrix. Additionally, our previous study showed that PDA can form composites with calcium silicate hydrate (C-S-H, primary cement hydration product), which enhances the mechanical properties of C-S-H [60]. The formation of this C-S-H-PDA also contributed to the superior compressive strength of the mortar containing Bio_PDA. The addition of 30 % Bio_PDA resulted in 2 % lesser strength than the control batch (without biochar) and 32 % higher strength than the Bio_Grn after 56 days. The lower strength of 30 % Bio_PDA samples compared to the 23 % Bio_PDA is due to the dilution effects.

The addition of 23 % Bio_PAA in mortar samples resulted in a higher strength compared to the control (without biochar), raw biochar (Bio_Control), and ground biochar (Bio_Grn) containing samples after 28 days of sealed curing. The strength improvement of Bio_PAA after long-term curing (i.e., 56 days) was attributed to the delayed hydration effect of this additive. As observed in Fig. 5(f), the workability of the Bio_PAA batch was higher compared to the Bio_Grn and Bio_Control, which enabled the formation of a denser matrix after the addition of Bio_PAA and hence resulted in a higher compressive strength.

3.3.2. *Effects on the crystalline phase formations*

The XRD patterns of the sealed-cured samples confirmed the presence of calcite, vaterite, calcium silicate phases (alite and belite), ettringite, gypsum, and portlandite (Fig. 9). Compared to the control batch, the sample containing Bio_Grn showed reduced intensity for portlandite and ettringite (Fig. 9(a)). The reduction in these typical cement hydration products is attributed to the dilution effect resulting from the replacement of binder with ground biochar. Similar reduction in the intensity of the hydration products was observed in the case of Bio_PDA and Bio_PAA batches as shown in Fig. 9(b) and Fig. 9(c), respectively. In addition to the dilution effect, the negative charges of PDA and PAA (Fig. 4(b)) capture the Ca^{2+} ions, hindering the formation of portlandite and ettringite in the matrix. However, Bio_Grn and Bio_-PDA batches showed higher intensity of different calcium carbonate polymorphs (i.e., calcite and vaterite) compared to the control batch. The formation of $CaCO_3$ in these samples is due to the presence of CO_2 in the atmosphere, indicating that adding biochar may have made these samples more vulnerable to atmospheric carbonation.

3.3.3. *Effects on the bound water contents*

The thermal analysis plots for paste samples containing various functionalized biochar after 28 days of sealed curing is presented in Fig. 10(a). The weight loss below 105°C corresponds to the dehydration of C-S-H and ettringite, the dehydration of AFm occurs at 100°C–200°C, 400°C–500°C is the range for the decomposition of portlandite and carbonates decomposes above 550°C [44,59–61].

Fig. 10(a) reveals that the decomposition up to 200°C is relatively higher for the control batch, indicating that the control batch produced more hydrated products than the biochar batches. As a result of the dilution effect, the total amount of hydrated products (C-S-H, AFm) is comparatively lower for biochar batches than the control batch. As observed from Fig. 10(a), the biochar containing batches showed a broad weight loss peak within the temperature range of 450–700°C. This relatively gradual weight loss is due to the decomposition of biochar (visible in Fig. 2) as well as the dehydration of C-S-H. Fig. 10(b) represents the chemically bound water and weight loss due to the biochar decomposition for different batches. The chemically bound water and biochar decomposition were measured by considering the weight loss between the range of 105°C–600°C. The weight losses due to the biochar decomposition (Fig. 2) were 2.79 % and 3.51 % for 23 % and 30 % biochar batches, respectively, within the same temperature range. The amount of chemically bound water was lowest for Bio_Grn batches, whereas it was higher for Bio_PDA and Bio_PAA batches compared to the Bio_Grn batches. Lesser amounts of chemically bound water content in the biochar containing batches were expected due to the dilution effect.

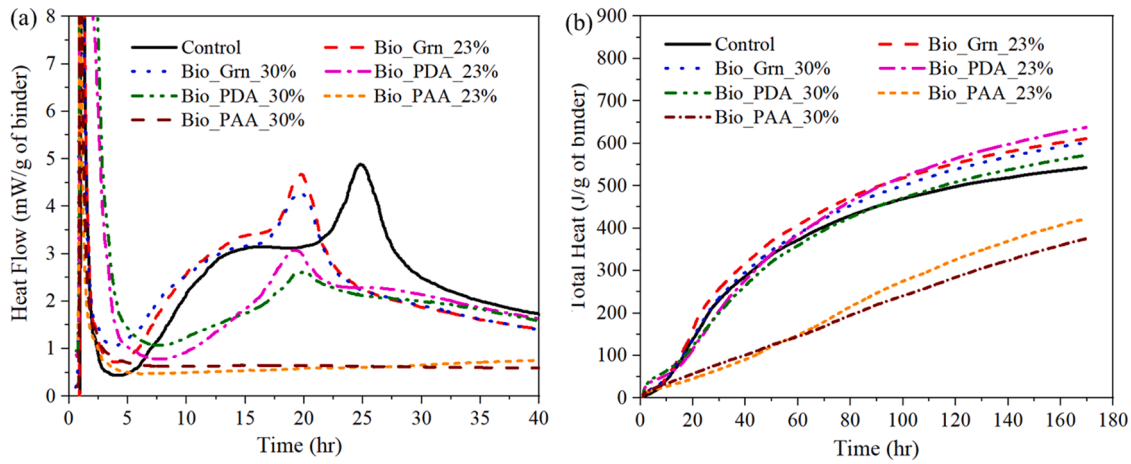

Fig. 7. (a) Heat flow and (b) total heat release for the paste mixtures containing functionalized biochar batches.

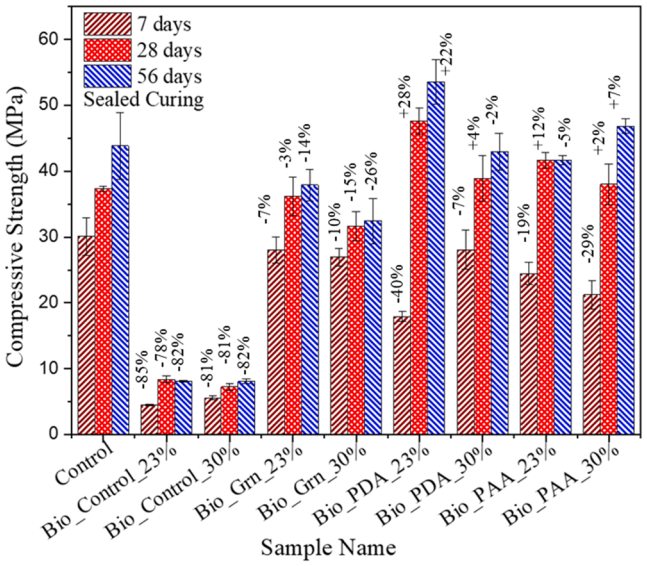

Fig. 8. Compressive strength of mortar samples exposed to sealed curing for various durations.The data labels show % difference with respect to the strength of the control samples after the same curing duration.

3.4. Effects of functionalized biochar in carbonation curing system

3.4.1. Role in compressive strength

The compressive strength of the mortar samples containing various dosages of functionalized biochar and exposed to carbonation curing are shown in Fig. 11. The compressive strength of the control batch (without biochar) exposed to carbonation curing was lower than that achieved in the case of sealed curing after the same curing duration. Noteworthy, for this study, the binder mixture contained a blend of OPC and slag cement in a 1:1 ratio. Such blended binders with high SCM dosage are likely to form a very small amount of portlandite. As a result, when these samples are exposed to long-term carbonation curing, as in this study, the C-S-H starts decalcifying, which caused poorer strength compared to the sealed cured control sample. This prolonged carbonation leads to moisture starvations, increasing porosity, and degraded binder gel structure, which negatively affects strength development [62].

Similar to the sealed cured batch, the addition of raw biochar drastically reduced the compressive strengths of the mortars. Specifically, the Bio_Control batches showed a compressive strength of around 5 MPa after 56 days of carbonation curing, confirming that such samples containing direct use of raw biochar are unlikely to be useful for load-bearing applications. However, the addition of functionalized biochar significantly enhanced their effects on the compressive strength of the mortar samples. Specifically, at a 23 % dosage level, all of the mortar samples containing functionalized biochar resulted in a higher compressive strength compared to the control batch (without biochar) after 56 days of carbonation curing. The highest strength after 56 days of carbonation curing was 43 MPa for the 23 % Bio_PDA sample, which was 24 % higher than the control batch. Among the batches containing functionalized biochar, only the Bio_PAA at 30 % dosage showed slightly lesser (2%) strength than the control batch. To further understand the role of these functionalized biochar on the strength, microstructural studies were performed.

3.4.2. Effects on the crystalline phase formations

The XRD patterns of the paste samples containing various functionalized biochar are shown in Fig. 12. Calcite was the primary phase present in these samples in addition to vaterite and calcium silicate phases (i.e., alite and belite). The control batch showed the highest peak intensity for calcite compared to the biochar batches, regardless of the biochar processing and dosages. In addition to the dilution effect, the inclusion of biochar hinders the carbonation process by making the matrix denser, resulting in low calcite formation in the case of accelerated carbonation curing. Similar to the calcite observation, the vaterite peak was also higher in the control batch.

3.4.3. Effects on the carbonate formation

The thermal analysis plots of the 28 days carbonation cured samples with various dosages biochar are shown in Fig. 13. It is evident from this figure that the weight loss associated with dehydration up to 200°C was relatively higher for the biochar containing batches compared the control batch, indicating that biochar batches contained more hydrated phases compared to the control batch [63]. This is because of the water retention capacity of biochar within the pores, which can improve the long-term hydration properties of the samples [64,65]. Fig. 13(b) presents the total calcium carbonate content (%) without biochar adjustment and with biochar adjustment. In 100 g of paste sample, the amount of biochar is 12.92 g and 16.22 g for 23 % and 30 % biochar batches, respectively. From Fig. 2, it is observed that the weight loss due to the biochar decomposition is 23.98 % within the same temperature range (550–900°C). Then Eq. 3 is used to calculate the decomposition of biochar in Fig. 13(a). According to the calculation, the weight loss due to the biochar decomposition was obtained 3.09 % and 3.89 % for 23 % and 30 % biochar batches, respectively. Then finally, Eq. 2 is used to determine the $CaCO_3$ with biochar adjustment (detailed calculation is given in supplementary section Table S1). Fig. 13(b) shows that the control batch had the highest $CaCO_3$ content compared to the biochar

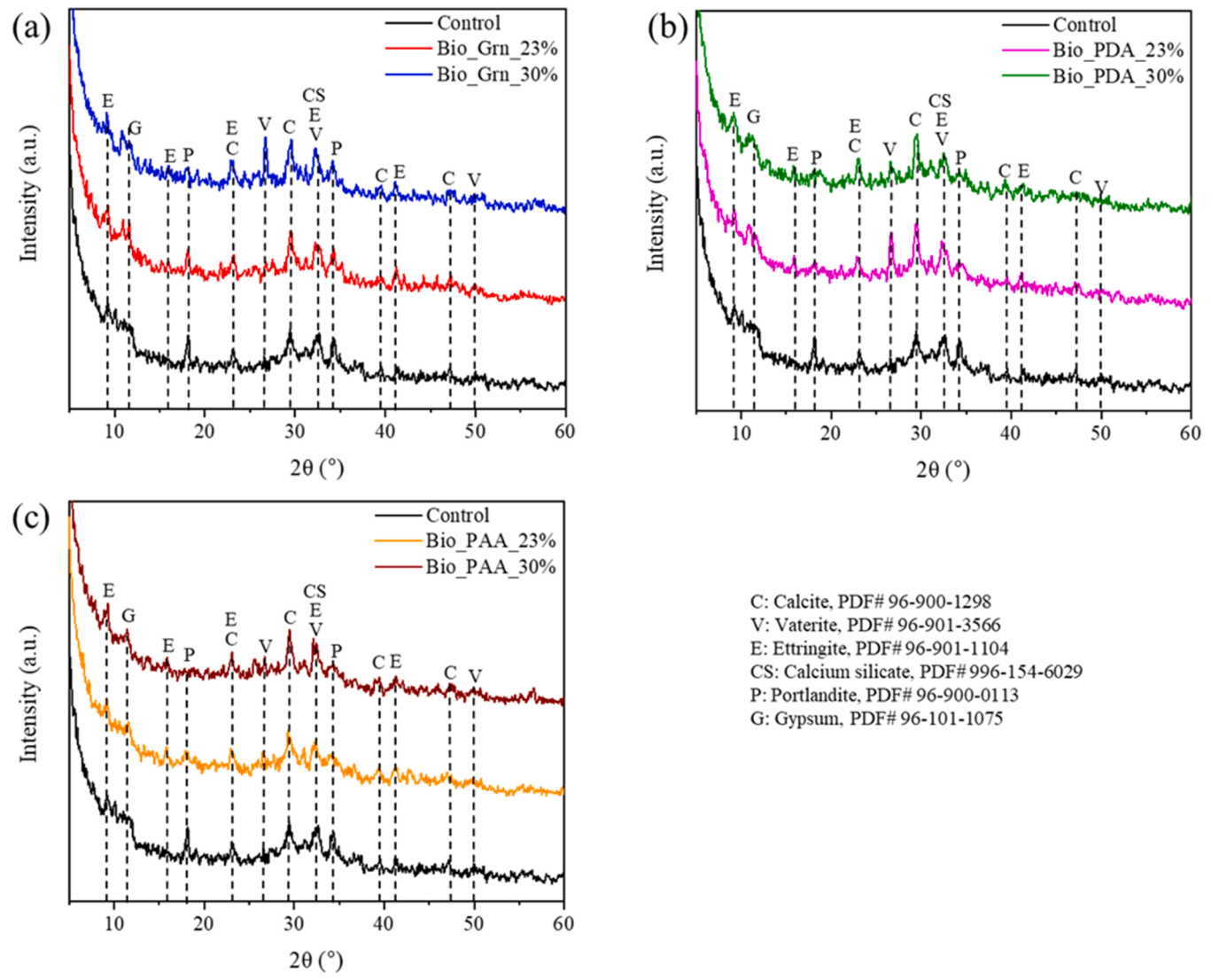

Fig. 9. X-ray diffraction (XRD) plots of 28 days sealed cured samples.

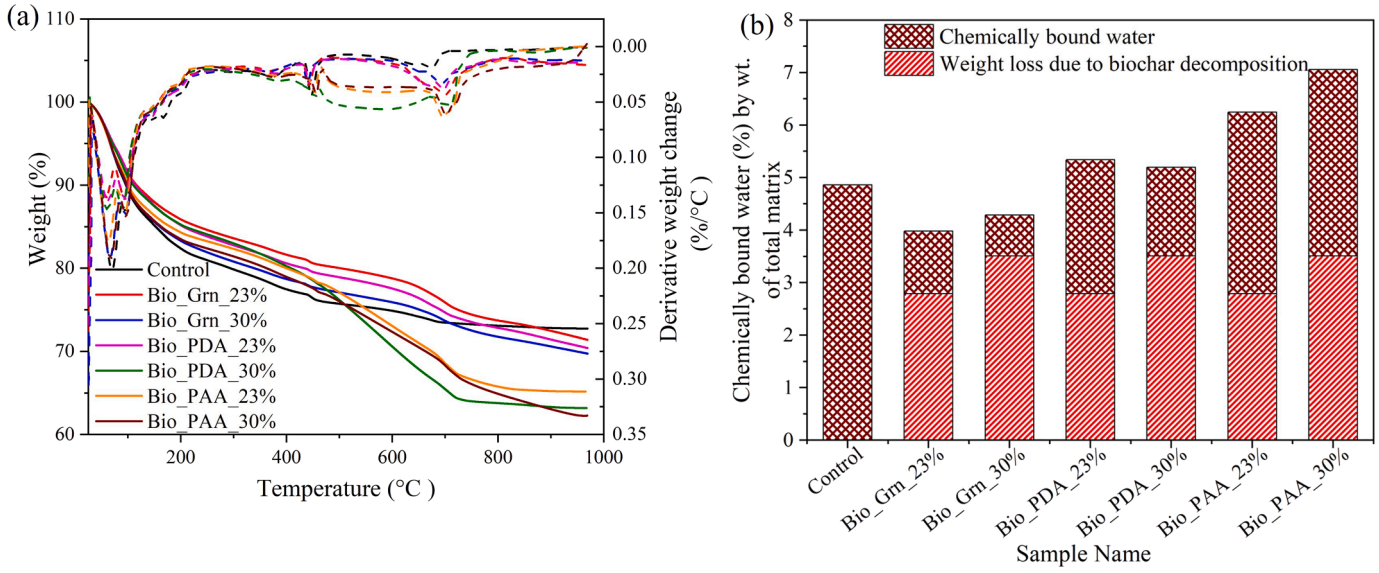

Fig. 10. (a): Thermogravimetric analysis (TGA) plots of 28 days sealed cured samples and (b) bar chart showing the weight loss (%) in samples from 105℃ to 600℃.

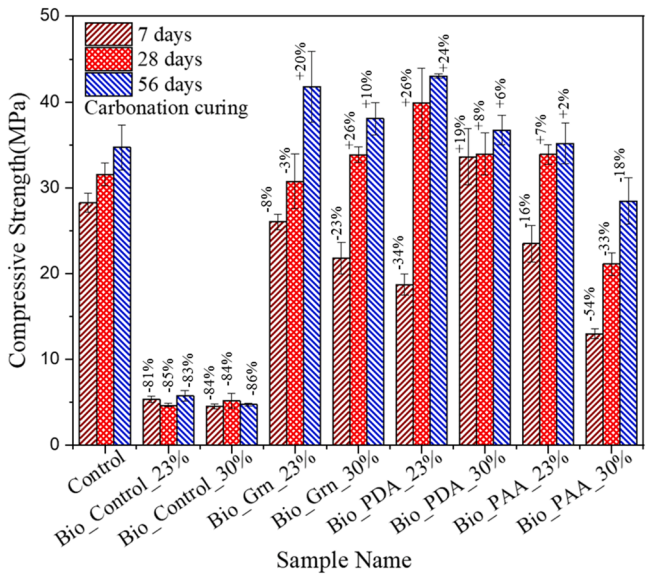

Fig. 11. Compressive strength of mortar samples exposed to carbonation curing for various durations. The data labels show % difference with respect to the strength of the control samples after the same curing duration.

containing batches, matching the observations from XRD in Fig. 12. Such reduced amounts of $CaCO_3$ formation in the biochar containing batches are primarily due to the dilution effect. However, the addition of these biochar samples hindered the carbonation of the matrix. This denser cement matrix inhibited CO_2 from entering the system (diffusion) during the carbonation curing process. As a result, total weight loss due to the decomposition of $CaCO_3$ was comparatively lower for the biochar batches. The $CaCO_3$ content for Bio_PAA_30 % was the lowest compared to the other batches due to the limited diffusion of CO_2, which also resulted in the poor compressive strength of this batch.

3.5. Dispersion of biochar in cementitious system

Due to the low density, the uniform dispersion of biochar in binder mixtures can be challenging. Therefore, to evaluate the dispersion of the functionalized biochar in the binder mixture, BSE images with elemental mapping were collected. Fig. 14(a) and Fig. 14(c) illustrate the low- and high-resolution BSE images, and Fig. 14(b) and Fig. 14(d) represent carbon element mapping showing the biochar distribution in the hardened matrix for the sample containing 23 % Bio_PDA. As observed from these images, biochar was uniformly distributed throughout the matrix for the Bio_PDA sample. Similar images were collected for the Bio_Grn and Bio_PAA containing samples (supplementary Figure S1 and Figure S2), which ensured uniform biochar distribution in these samples as well.

Fig. 15 shows the interaction between the biochar and cement matrix in the paste sample. In this figure, the dark grey area indicated by EDS data point (b) was mainly composed of Ca and Si, which represents the formation of the C-S-H phase, whereas the bright grey area (EDS data point (d)) represented the unreacted C_3S and C_2S. The EDS data points (c) and (e) show the interaction between the binder and biochar particles. These are primarily composed of Ca, Si, Al, C, and O, indicating that C-S-H and $CaCO_3$ were formed around the biochar, which increased the bonding between binder and biochar particles. Moreover, biochar particles formed needle-like shapes after the ball milling, as marked in Fig. 15(a). Based on an image analysis, the aspect ratio of these needle-shaped biochar was 6.5. The formation of such needle-shaped biochar particles can serve as a micro-reinforcement and can further contribute to the strength enhancement by crack bridging.

3.6. Role of functionalized biochar on the environmental impact

The biochar utilized in this study was derived by pyrolyzing Beetle-killed wood, fire-damaged trees, and other woody materials. According to the manufacturer, it contained 87.4 % carbon (by total dry mass), resulting in a CO_2 sequestration capacity of 3.2 kg CO_2 equivalent per kilogram of biochar. However, a more representative carbon footprint for wood waste-based biochar was considered, using global warming potential (GWP) data from various literature sources for analysis in this study. Previous studies showed that among various waste biomasses, wood waste-based biochar (WWB) has the highest carbon content because of having higher lignocellulose, with a maximum of 90.5 % [18,66], and their carbon sequestration potential can vary from −2740.10 to −1513.07 kg CO_2 eq per ton [18]. Calculating the net greenhouse gas (GHG) impact for each biochar unit involved combining the total CO_2 sequestration from the biochar with the corresponding CO_2 emissions resulting from its production.

Biochar production primarily comprises two main stages: feedstock pretreatment and biochar preparation; feedstock pretreatment includes drying, storage, grinding, chipping, or pelletizing [18]. Conversely, the carbon emission due to the biochar preparation process depends on the sources of power used to operate the pyrolysis plant. Puettmann et al. conducted an evaluation of the environmental impact associated with biochar production from forest residues using three portable systems, namely biochar solutions incorporated (BSI), Oregon Kiln, and air-curtain burner [46]. Within the BSI system, various power sources were utilized, including grid connection for in-town locations and a diesel or gasifier-based generator for near-forest locations [20,46], while another study incorporated natural gas for pyrolyzing wood sawdust [29]. These studies considered the biogenic carbon emissions released during biochar production to be equal to the CO_2 absorbed during tree growth [29,46]. Depending on the system used (e.g., gasifier-based generator or diesel-based generator), CO_2 emissions from biochar production range from 0.2 to 0.8 kg CO_2 eq/kg biochar [46]. Conversely, the carbon sequestration potential of these biochars varies from 2.6 to 3 kg CO_2 eq/kg biochar [46]. The total CO_2 emissions during biochar production and the CO_2 sequestered within were combined to calculate the net GWP per kg of biochar. Diverse net GWP data for biochar production gathered from various sources, as depicted in Table 5, were employed to illustrate the range of carbon footprints associated with mortar production when biochar is integrated into the process. Polyacrylic acid (PAA) and polydopamine (PDA) were added during grinding to enhance the workability of biochar. The GWP of PAA was obtained from SimaPro (Table 4), but due to a lack of specific data, the GWP for PDA was assumed to be the same as that of PAA.

The primary focus was establishing the functional unit as the mass of binder needed per cubic meter of mortar, subsequently calculating the other raw material quantities for the same mortar sample and summing them up. Fig. 16 shows the GWP of different biochar-based mortar samples and their corresponding compressive strength and compares them with the biochar-excluded control batch. Nearly all biochar batches subjected to carbonation curing exhibited negative carbon footprints, with GWP reductions ranging from 90 % to 170 % compared to the control batch (Fig. 16(a)). Prior research indicated that increased biochar incorporation in mortar typically results in reduced compressive strength [5]; nevertheless, this study demonstrates that even with the addition of 23 % biochar by the weight of the binder, compressive strengths of up to 43 MPa was attained in a carbonation system and up to 54 MPa when samples were cured under sealed conditions. Therefore, achieving a greater reduction in carbon footprint without compromising compressive strength is possible. Moreover, an increase in biochar dosage from 23 % to 30 % resulted in a reduction in carbon footprint, while the compressive strength of the 23 % biochar-containing mortar sample remained higher. Bio_Control and Bio_Grn, with similar mix compositions (excluding the grinding energy for Bio_Grn), exhibit comparable carbon footprints; however, Bio_Control's compressive

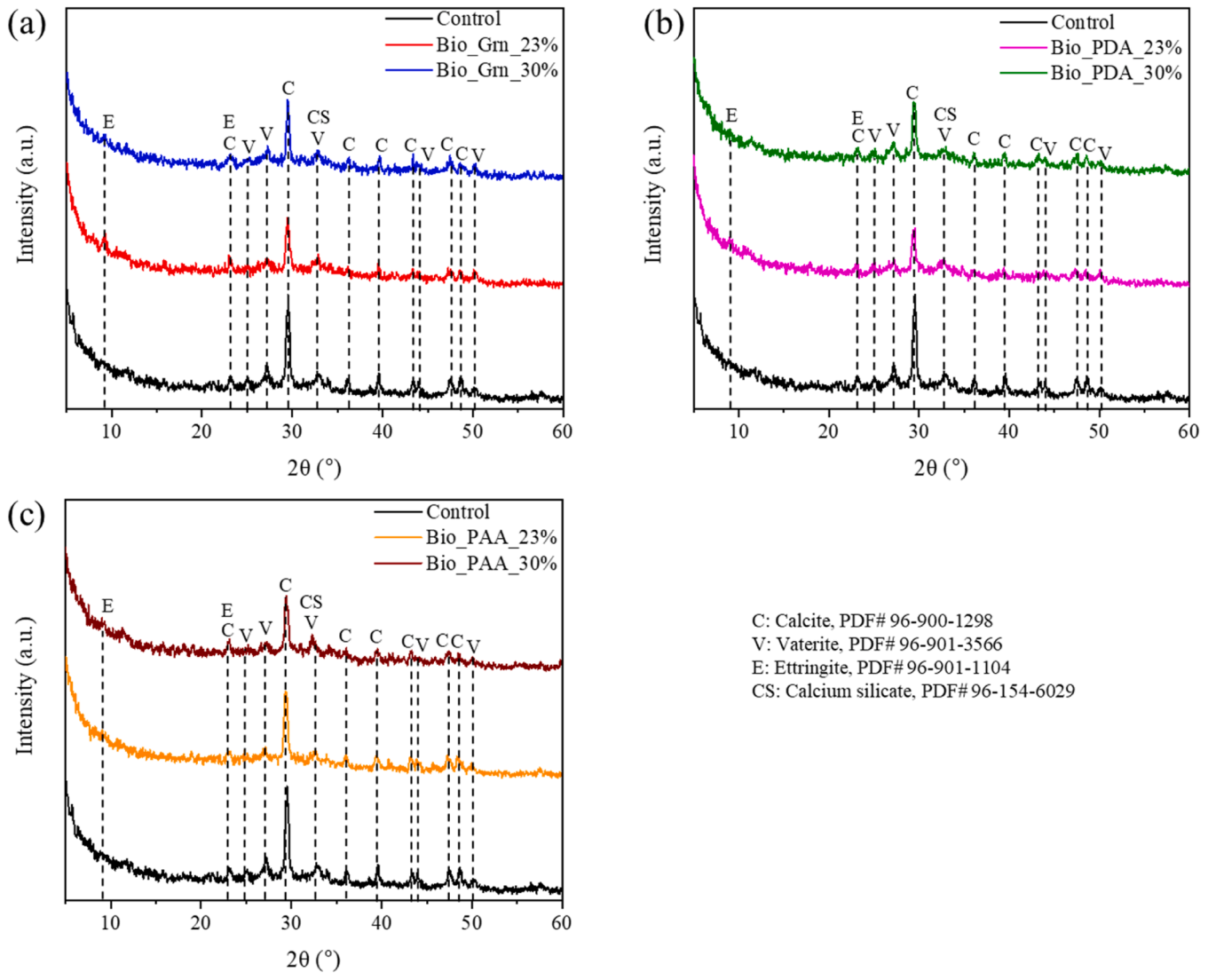

Fig. 12. X-ray diffraction (XRD) plots for 28 days carbonation cured samples.

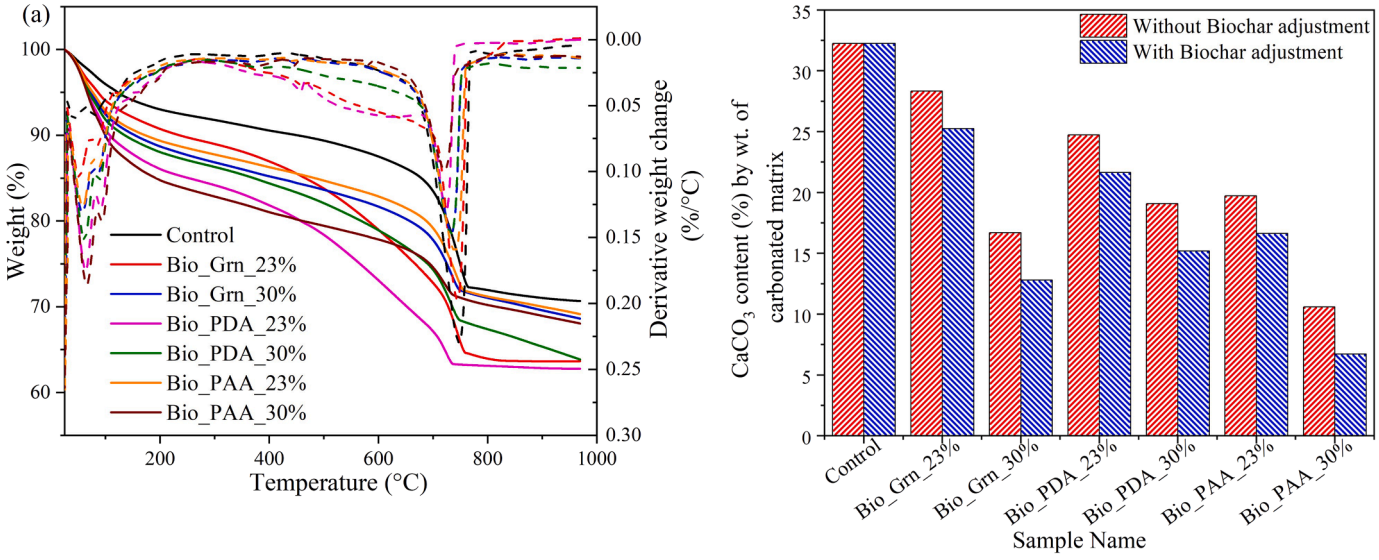

Fig. 13. (a) Thermogravimetric analysis (TGA) plots of carbonation curing 28 days paste samples, (b) bar chart showing calcium carbonate contents (%) with respect to the total carbonated matrix.

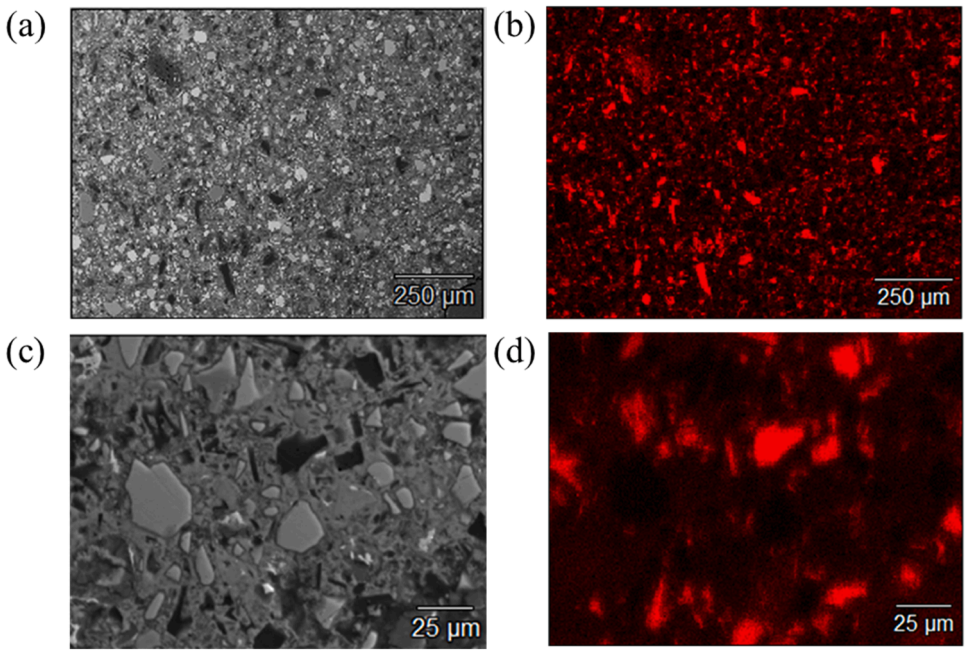

Fig. 14. (a) Low-resolution BSE image, (b) low-resolution BSE area mapping, (c) high-resolution BSE image, and (d) high-resolution BSE area mapping of Bio_-PDA_23 % carbonation curing batch showing carbon distribution in the matrix.

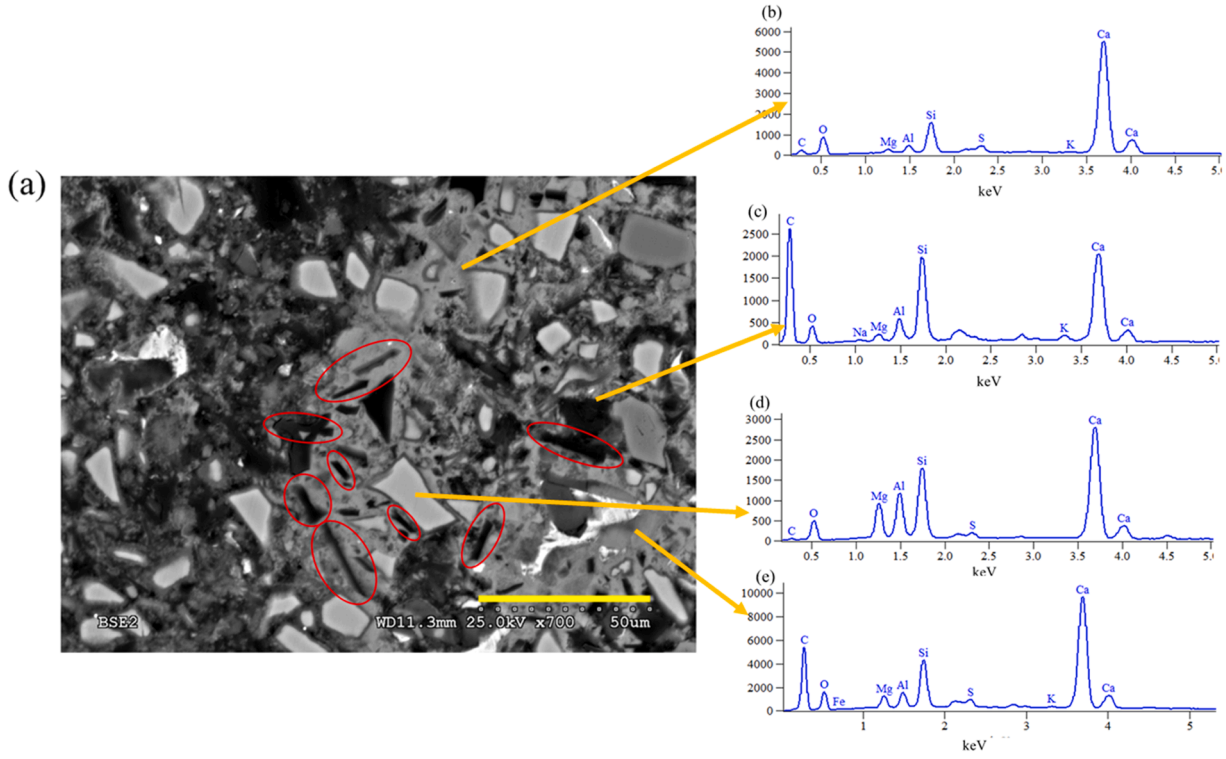

Fig. 15. High-resolution BSE image of 28-day carbonation curing Bio_PAA_23 % batch: (a) the shape of biochar (aspect ratio), and (b)-(e) EDS data points showing C-S-H composition.

strength is 75–85 % lower than that of Bio_Grn for both carbonation-cured and sealed-cured mixes.

For sealed-cured samples as shown in Fig. 16(b), the addition of 23 % biochar may not consistently achieve carbon negativity; however, ensuring this outcome is possible by increasing the percentage of biochar addition to 30 %. Like the carbonation-cured mixes, the 23 % biochar batch exhibited a lower GWP reduction but a higher compressive strength. Moreover, due to the additional CO_2 sequestration in the carbonation-cured samples, their carbon footprint consistently remained lower than that of the sealed-cured samples. Lastly, the GWP of mixes containing PDA and PAA was relatively higher compared to other biochar-containing mixes, attributed to the additional carbon footprint introduced by the two additives.

From the above discussion, it is certain that there is a correlation

Table 5
Net GWP data per kg of biochar.

Reference	Production emission (kg CO_2 eq/kg biochar)	Carbon sequestration (kg CO_2 eq/kg biochar)	Net GWP (kg CO_2 eq/kg biochar)
[66]	0.7	−2.6	−1.9
[46]	0.8	−3	−2.2
[46]	0.2	−3	−2.8

between biochar dosage, GWP, and compressive strength. Hence, when assessing functional equivalence among binders with or without biochar addition, compressive strength should be regarded as a critical parameter. Consequently, a new functional unit was introduced as the mass of the binder needed per cubic meter of mortar or concrete to achieve 1 MPa of compressive strength (kg/(m^3.MPa)) [67,68]. The implication of this functional unit is that achieving comparable compressive strength requires varying the amount of binder needed per cubic meter, thereby influencing the carbon footprint. As depicted in Fig. 17, the carbon footprint of Bio_Control was the lowest among all the mixes containing biochar, while the compressive strength of these mixes ranged only from 4 to 8 MPa. The observed discrepancy arises because the low compressive strength necessitates an increased binder requirement, consequently elevating the carbon footprint. However, the increase in binder content also entails a higher demand for biochar, leading to substantial carbon negativity and ultimately resulting in a net reduction in carbon footprint. However, despite its low carbon footprint, the lack of workability and significantly low compressive strength make it unsuitable for being used as a mix. This is the same reason that the GWP of 30 % biochar-contained samples have a lower value despite having lower compressive strength. Nevertheless, carbon negativity was evident in all the biochar samples even when this new functional unit was applied.

4. Conclusion

This article presented an innovative approach to producing carbon-neutral/negative cementitious composites by engineering the interface

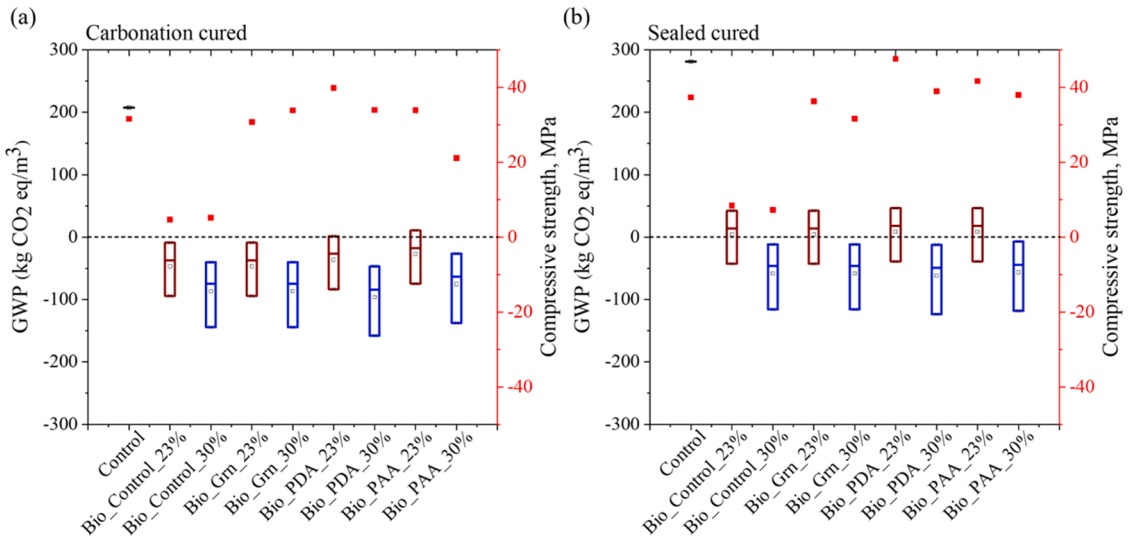

Fig. 16. Correlating GWP and compressive strength of biochar-based mortar samples- (a) carbonation cured, and (b) sealed cured.

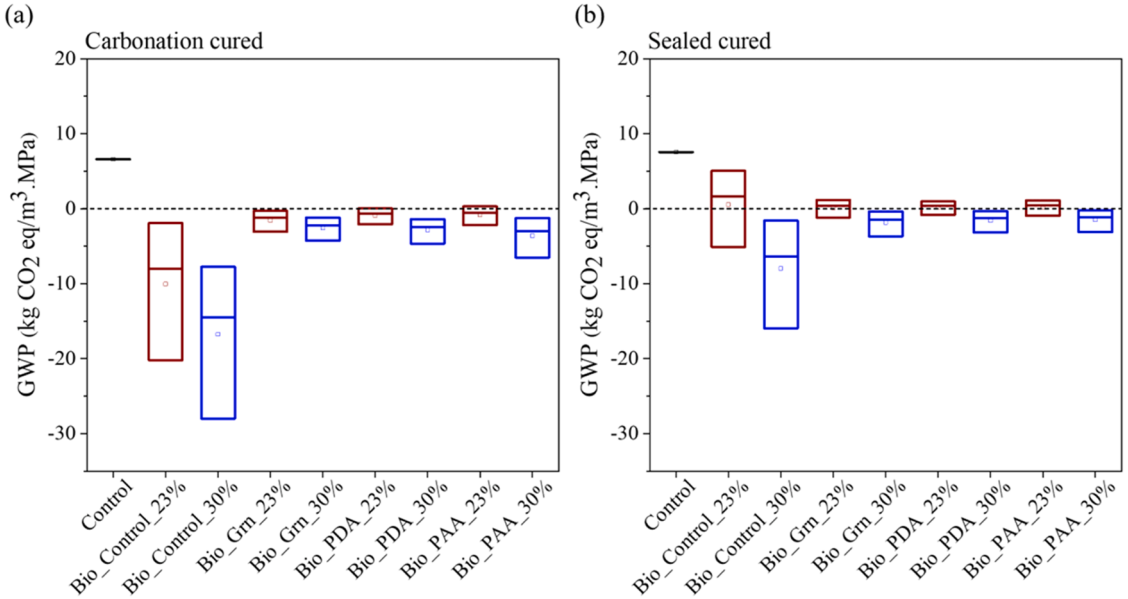

Fig. 17. GWP of (a) carbonation cured and (b) sealed cured samples considering compressive strength as a parameter of the functional unit.

between cement paste matrix and biochar using organic polymers. The following are the concluding remarks that can be drawn from the results of this study:

I. The carbon neutral/ negative cementitious composites produced using raw biochar was unworkable due to the high-water retention capacity of biochar. The compressive strength of these mixes were also very low. Compared to the raw biochar, the addition of functionalized biochar drastically (up to 63 %) improved the workability of the fresh mixtures.
II. The addition of ground biochar (Bio_Grn) accelerated the cement hydration by providing additional surface area for hydration products to nucleate. The polymer-modified functionalized biochar (Bio_PDA and Bio_PAA) suppressed cement hydration at an early age. However, after 7 days, Bio_PDA-containing batches showed the same or higher cement hydration heat compared to the control batch.
III. The use of functionalized biochar enables reducing the carbon footprint of cementitious composites up to 170 % after considering the GWP associated with all the raw ingredients, including biochar production and use of the organic polymers.
IV. This study showed a pathway to produce workable carbon-neutral (or net zero carbon) and carbon-negative cementitious composites. For the 56 days sealed curing environment, the maximum strength of the carbon-neutral batches was 54 MPa, which was achieved by using 23 % Bio_PDA. This strength was 22 % higher than the control batch produced without any biochar. For this curing condition, the maximum compressive strength for the carbon-negative batch was 47 MPa, achieved by using 30 % Bio_PAA. The use of this carbon-negative cementitious composite enables permanent sequestration of up to 120 kg CO_2 eq per m^3 of the structure constructed using this composite.
V. For carbonation curing, all the batches containing functionalized biochar were carbon-negative and showed reasonable compressive strength. The maximum compressive strength after 56 days of carbonation curing was 43 MPa, corresponding to the mortar sample containing 23 % Bio_PDA. This strength was 24 % higher than the traditional control batch, produced under the same curing condition, which also had a significantly high carbon footprint.

This study demonstrates the potential of using a higher dosage of functionalized biochar to achieve carbon neutral/negative cementitious composites with superior performance. Nevertheless, further exploration is required into various factors. This study utilized a specific type of biochar; however, biochar's derived from different feedstocks or processed under varying conditions could result in different performance characteristics, affecting both the workability and mechanical properties. More research is needed to generalize the findings to other biochar types. The demonstrated improvements in workability and mechanical performance with higher biochar dosages, bring us significantly closer to making carbon-neutral construction materials a practical reality. This progress sets a solid foundation for future innovations in sustainable building practices, with the potential for even greater advancements as these limitations are addressed.

CRediT authorship contribution statement

Warda Ashraf: Writing – review & editing, Supervision, Resources, Project administration, Methodology, Investigation, Funding acquisition, Formal analysis, Conceptualization. **Nishad Ahmed:** Writing – original draft, Investigation, Formal analysis, Data curation. **Adhora Tahsin:** Writing – original draft, Investigation, Formal analysis, Data curation. **Farzana Mustari Nishat:** Writing – original draft, Investigation, Formal analysis, Data curation.

Declaration of Competing Interest

The authors declare that they have no known competing financial interests or personal relationships that could have appeared to influence the work reported in this paper.

Acknowledgements

Funding for this research was provided by the US National Science Foundation (NSF # ECI -2028462, EFRI - 2318123). All opinions, findings, and conclusions or recommendations expressed in this material are those of the authors and do not necessarily reflect the views of the funding agencies.

Appendix A. Supporting information

Supplementary data associated with this article can be found in the online version at doi:10.1016/j.conbuildmat.2024.139143.

Data availability

Data will be made available on request.

References

[1] International Energy Agency, Assessing the Effects Of Economic Recoveries On Global Energy Demand And CO2 Emissions in 2021 Global Energy, 2021. (Online). www.iea.org/t&c/.
[2] BBC, Climate change: EU Leaders Set 55% Target for CO_2 Emissions Cut, Dec. 2023. (Online). https://www.bbc.com/news/world-europe-55273004. (Accessed 24 December 2023).
[3] BBC, Climate change: China Aims for 'Carbon Neutrality by 2060,' Sep. 22, 2020. (Online). https://www.bbc.com/news/science-environment-54256826. (Accessed 24 December 2023).
[4] United Nations, For a Livable Climate: Net-zero Commitments Must Be Backed by Credible Action. (Online). https://www.un.org/en/climatechange/net-zero-coalition.
[5] L. Chen, et al., Biochar-augmented carbon-negative concrete, Chem. Eng. J. 431 (2022), https://doi.org/10.1016/j.cej.2021.133946.
[6] J.A. Ober and U.S.G. Survey, Mineral commodity summaries 2018, Reston, VA, 2018. doi: 10.3133/70194932.
[7] L.D. Ellis, A.F. Badel, M.L. Chiang, R.J.Y. Park, Y.M. Chiang, Toward electrochemical synthesis of cement—An electrolyzer-based process for decarbonating $CaCO_3$ while producing useful gas streams, Proc. Natl. Acad. Sci. USA 117 (23) (2020) 12584–12591, https://doi.org/10.1073/pnas.1821673116.
[8] X. Lin, W. Li, Y. Guo, W. Dong, A. Castel, K. Wang, Biochar-Cement Concrete toward Decarbonisation and Sustainability for Construction: Characteristic, Performance and Perspective, J. Clean. Prod. (2023), https://doi.org/10.1016/j.jclepro.2023.138219.
[9] Z. Li, X. Shi, Towards sustainable industrial application of carbon-negative concrete: synergistic carbon-capture by concrete washout water and biochar, Mater. Lett. 342 (2023), https://doi.org/10.1016/j.matlet.2023.134368.
[10] Y. Zhang, et al., Biochar as Construction Materials for Achieving Carbon Neutrality, Springer, 2022, https://doi.org/10.1007/s42773-022-00182-x.
[11] D. Winters, K. Boakye, S. Simske, Toward carbon-neutral concrete through biochar–cement–calcium carbonate composites: a critical review, Sustainability 14 (8) (2022), https://doi.org/10.3390/su14084633.
[12] S. Sri Shalini, K. Palanivelu, A. Ramachandran, V. Raghavan, Biochar from Biomass Waste as a Renewable Carbon Material for Climate Change Mitigation in Reducing Greenhouse Gas Emissions—a Review, Springer Science and Business Media Deutschland GmbH (2021), https://doi.org/10.1007/s13399-020-00604-5.
[13] J.E. Korb, N.C. Johnson, W.W. Covington, Slash pile burning effects on soil biotic and chemical properties and plant establishment: recommendations for amelioration, Restor. Ecol. 12 (1) (2004) 52–62, https://doi.org/10.1111/j.1061-2971.2004.00304.x.
[14] M.T. Moreira, I. Noya, G. Feijoo, The Prospective Use of Biochar as Adsorption Matrix – a Review From a Lifecycle Perspective, Bioresour. Technol. (2017), https://doi.org/10.1016/j.biortech.2017.08.041.
[15] H.P. Schmidt, et al., Pyrogenic Carbon Capture and Storage, Blackwell Publishing Ltd. (2019), https://doi.org/10.1111/gcbb.12553.
[16] A. Papageorgiou, E.S. Azzi, A. Enell, C. Sundberg, Biochar produced from wood waste for soil remediation in Sweden: Carbon sequestration and other environmental impacts, Sci. Total Environ. 776 (2021), https://doi.org/10.1016/j.scitotenv.2021.145953.
[17] D. Iribarren, J.F. Peters, J. Dufour, Life cycle assessment of transportation fuels from biomass pyrolysis, Fuel 97 (2012) 812–821, https://doi.org/10.1016/j.fuel.2012.02.053.

[18] F. Xia, Z. Zhang, Q. Zhang, H. Huang, X. Zhao, Life Cycle Assessment of Greenhouse Gas Emissions for Various Feedstocks-based Biochars as Soil Amendment, Sci. Total Environ. 10 (2024), https://doi.org/10.1016/j.scitotenv.2023.168734.

[19] L. Zampori, G. Dotelli, V. Vernelli, Life cycle assessment of hemp cultivation and use of hemp-based thermal insulator materials in buildings, Environ. Sci. Technol. 47 (13) (2013) 7413–7420, https://doi.org/10.1021/es401326a.

[20] K. Sahoo, A. Upadhyay, T. Runge, R. Bergman, M. Puettmann, E. Bilek, Life-cycle assessment and techno-economic analysis of biochar produced from forest residues using portable systems, Int J. Life Cycle Assess. (2020) 189–213, https://doi.org/10.1007/s11367-020-01830-9/Published.

[21] A.V. McBeath, C.M. Wurster, M.I. Bird, Influence of feedstock properties and pyrolysis conditions on biochar carbon stability as determined by hydrogen pyrolysis, Biomass-.-. Bioenergy 73 (2015) 155–173, https://doi.org/10.1016/j.biombioe.2014.12.022.

[22] J. Lehmann, J. Gaunt, M. Rondon, Bio-char Sequestration in Terrestrial Ecosystems -a Review in Mitigation and adaptation strategies for global change 11 (2006): 403-427, doi: 10.1007/s11027-005-9006-5.(2006).

[23] P. Leturcq, GHG displacement factors of harvested wood products: the myth of substitution, Sci. Rep. 10 (1) (2020), https://doi.org/10.1038/s41598-020-77527-8.

[24] H.W. Kua, S. Gupta, A.N. Aday, W.V. Srubar, Biochar-immobilized bacteria and superabsorbent polymers enable self-healing of fiber-reinforced concrete after multiple damage cycles, Cem. Concr. Compos 100 (2019) 35–52, https://doi.org/10.1016/j.cemconcomp.2019.03.017.

[25] L. Wang, et al., Biochar as green additives in cement-based composites with carbon dioxide curing, J. Clean. Prod. 258 (2020) 120678, https://doi.org/10.1016/j.jclepro.2020.120678.

[26] D. Suarez-riera, L. Restuccia, G.A. Ferro, The use of Biochar to reduce the carbon footprint of cement-based materials, Procedia Struct. Integr. 26 (2020) 199–210, https://doi.org/10.1016/j.prostr.2020.06.023.

[27] A. Dixit, S. Gupta, S. Dai, H. Wei, Waste Valorisation using biochar for cement replacement and internal curing in ultra-high performance concrete, J. Clean. Prod. 238 (2019) 117876, https://doi.org/10.1016/j.jclepro.2019.117876.

[28] S. Gupta, H.W. Kua, Effect of water entrainment by pre-soaked biochar particles on strength and permeability of cement mortar, Constr. Build. Mater. 159 (2018) 107–125, https://doi.org/10.1016/j.conbuildmat.2017.10.095.

[29] S. Gupta, H.W. Kua, C.Y. Low, Use of biochar as carbon sequestering additive in cement mortar, Cem. Concr. Compos 87 (2018) 110–129, https://doi.org/10.1016/j.cemconcomp.2017.12.009.

[30] S. Gupta, H.W. Kua, H.J. Koh, Application of biochar from food and wood waste as green admixture for cement mortar, Sci. Total Environ. 619–620 (2018) 419–435, https://doi.org/10.1016/j.scitotenv.2017.11.044.

[31] S. Gupta, H.W. Kua, Carbonaceous micro-filler for cement: Effect of particle size and dosage of biochar on fresh and hardened properties of cement mortar, Sci. Total Environ. 662 (2019) 952–962, https://doi.org/10.1016/j.scitotenv.2019.01.269.

[32] H.J. Cha, D.S. Hwang, S. Lim, Development of bioadhesives from marine mussels, Biotechnology Journal: Healthcare Nutrition Technology 3 (5) (2008) 631–638, https://doi.org/10.1002/biot.200700258.

[33] J.J. Wilker, The iron-fortified adhesive system of marine mussels, Angew. Chem. - Int. Ed. 49 (44) (2010) 8076–8078, https://doi.org/10.1002/anie.201003171.

[34] Z. Liu, et al., Effect of polydopamine on the biomimetic mineralization of mussel-inspired calcium phosphate cement in vitro, Mater. Sci. Eng. C. 44 (2014) 44–51, https://doi.org/10.1016/j.msec.2014.07.063.

[35] R.I. Khan, M.I. Haque, W. Ashraf, S. Shah, N. Saleh, Role of biopolymers in enhancing multiscale characteristics of carbonation-cured cementitious composites, Cem. Concr. Compos 134 (2022), https://doi.org/10.1016/j.cemconcomp.2022.104766.

[36] Y. Fang, J. Wang, X. Qian, L. Wang, G. Lin, Z. Liu, Bio-inspired functionalization of very fine aggregates for better performance of cementitious materials, Constr. Build. Mater. 241 (2020), https://doi.org/10.1016/j.conbuildmat.2020.118104.

[37] P. Chen, et al., Bio-inspired functionalization of crumb rubber using polydopamine to enhance the performance of rubberized mortars, Constr. Build. Mater. 407 (2023), https://doi.org/10.1016/j.conbuildmat.2023.133550.

[38] Y. Guo, et al., Effect of polyacrylic acid emulsion on fluidity of cement paste, Colloids Surf. A Physicochem Eng. Asp. 535 (2017) 139–148, https://doi.org/10.1016/j.colsurfa.2017.09.039.

[39] M.I. Haque, R.I. Khan, W. Ashraf, H. Pendse, Production of sustainable, low-permeable and self-sensing cementitious composites using biochar, Sustain. Mater. Technol. 28 (2021) e00279, https://doi.org/10.1016/j.susmat.2021.e00279.

[40] ASTM C305, Standard Practice for Mechanical Mixing of Hydraulic Cement Pastes and Mortars of Plastic Consistency, 2009. (Online). www.astm.org.

[41] ASTM C1437, Standard Test Method for Flow of Hydraulic Cement Mortar, 2007. (Online). www.astm.org.

[42] ASTM C109, Standard Test Method for Compressive Strength of Hydraulic Cement Mortars (Using 2-in. or [50-mm] Cube Specimens), 2009. (Online). www.astm.org,

[43] ASTM C138, Standard Test Method for Density (Unit Weight), Yield, and Air Content (Gravimetric) of Concrete, 2008. (Online). www.astm.org,

[44] Karen, Scrivener, Ruben. Snellings, and Barbara. Lothenbach. A Practical Guide to Microstructural Analysis of Cementitious Materials, CRC Press, 2016.

[45] W. Ashraf, J. Olek, Carbonation behavior of hydraulic and non-hydraulic calcium silicates: potential of utilizing low-lime calcium silicates in cement-based materials, J. Mater. Sci. 51 (13) (2016) 6173–6191, https://doi.org/10.1007/s10853-016-9909-4.

[46] M. Puettmann, K. Sahoo, K. Wilson, E. Oneil, Life cycle assessment of biochar produced from forest residues using portable systems, J. Clean. Prod. 250 (2020), https://doi.org/10.1016/j.jclepro.2019.119564.

[47] S.K. Das, G.K. Ghosh, R.K. Avasthe, K. Sinha, Compositional heterogeneity of different biochar: effect of pyrolysis temperature and feedstocks, J. Environ. Manag. 278 (Jan. 2021), https://doi.org/10.1016/j.jenvman.2020.111501.

[48] S. Gupta, A. Kashani, A.H. Mahmood, Carbon sequestration in engineered lightweight foamed mortar – Effect on rheology, mechanical and durability properties, Constr. Build. Mater. 322 (2022), https://doi.org/10.1016/j.conbuildmat.2022.126383.

[49] S. Gupta, H.W. Kua, S.D. Pang, Biochar-mortar composite: manufacturing, evaluation of physical properties and economic viability, Constr. Build. Mater. 167 (2018) 874–889, https://doi.org/10.1016/j.conbuildmat.2018.02.104.

[50] Yun, W. Chang, H.D. Lee, J. Yeon, Mechanical properties of mortar containing bio-char from pyrolysis, J. Korean Soc. Struct. Diagn. Maint. Eng. 5 (2012) 67–74, https://doi.org/10.11112/JKSMI.2012.16.3.067.

[51] S. Mindess. Developments in the Formulation and Reinforcement of Concrete, second ed., Woodhead Publishing, 2019.

[52] M. Bouasker, P. Mounanga, P. Turcry, A. Loukili, A. Khelidj, Chemical shrinkage of cement pastes and mortars at very early age: Effect of limestone filler and granular inclusions, Cem. Concr. Compos 30 (1) (2008) 13–22, https://doi.org/10.1016/j.cemconcomp.2007.06.004.

[53] A. Goldman, A. Bentur, The influence of microfillers on enhancement of concrete strength, Cem. Concr. Res 23 (1993) 962–972, https://doi.org/10.1016/0008-8846(93)90050-J.

[54] A.M. Poppe, G. De Schutter, Cement hydration in the presence of high filler contents, Cem. Concr. Res 35 (12) (2005) 2290–2299, https://doi.org/10.1016/j.cemconres.2005.03.008.

[55] R. Duval, E.H. Kadri, Influence of fine and Ultrafine Particles on the Heat of Hydration and the Compressive Strength of Cement Mortars, 28, WIT Press, 2000.

[56] H. Maljaee, R. Madadi, H. Paiva, L. Tarelho, V.M. Ferreira, Incorporation of Biochar in Cementitious Materials: a Roadmap of Biochar Selection, Constr. Build. Mater. (2021), https://doi.org/10.1016/j.conbuildmat.2021.122757.

[57] Z. Gu, et al., Bio-inspired polydopamine modification of recycled carbon fibers for improving the performance of recycled carbon fiber reinforced mortars, Constr. Build. Mater. 414 (2024) 1–12, https://doi.org/10.1016/j.conbuildmat.2024.134912.

[58] J.S. Lota, Ã.K. Kendall, J. Bensted, Mechanism for the modification of Portland cement hydration using polyacrylic acid, Advances in Cement Research vol. No. 2, (1999) 45–56, https://doi.org/10.1680/adcr.2000.12.2.45.

[59] B. Ma, Y. Peng, H. Tan, Z. Lv, X. Deng, Effect of polyacrylic acid on rheology of cement paste plasticized by polycarboxylate superplasticizer, Materials 11 (7) (2018), https://doi.org/10.3390/ma11071081.

[60] M.I. Haque, I.B. Borno, R.I. Khan, W. Ashraf, Reducing carbonation degradation and enhancing elastic properties of calcium silicate hydrates using biomimetic molecules, Cem. Concr. Compos 136 (2023), https://doi.org/10.1016/j.cemconcomp.2022.104888.

[61] P. Nielsen, M.A. Boone, L. Horckmans, R. Snellings, M. Quaghebeur, Accelerated carbonation of steel slag monoliths at low CO_2 pressure - microstructure and strength development, J. CO2 Util. 36 (2020) 124–134, https://doi.org/10.1016/j.jcou.2019.10.022.

[62] S. Gupta, A. Kashani, A.H. Mahmood, T. Han, Carbon sequestration in cementitious composites using biochar and fly ash – Effect on mechanical and durability properties, Constr. Build. Mater. 291 (2021), https://doi.org/10.1016/j.conbuildmat.2021.123363.

[63] J. Liu, et al., Carbonation of steel slag at low CO_2 concentrations: novel biochar cold-bonded steel slag artificial aggregates, Sci. Total Environ. 902 (2023), https://doi.org/10.1016/j.scitotenv.2023.166065.

[64] A. Sirico, et al., Biochar from wood waste as additive for structural concrete, Constr. Build. Mater. 303 (2021), https://doi.org/10.1016/j.conbuildmat.2021.124500.

[65] A. Sirico, et al., Effects of biochar addition on long-term behavior of concrete, Theor. Appl. Fract. Mech. 122 (2022), https://doi.org/10.1016/j.tafmec.2022.103626.

[66] E.S. Azzi, E. Karltun, C. Sundberg, Prospective life cycle assessment of large-scale biochar production and use for negative emissions in stockholm, Environ. Sci. Technol. 53 (14) (2019) 8466–8476, https://doi.org/10.1021/acs.est.9b01615.

[67] A. Sagastume Gutiérrez, J.J. Cabello Eras, C.A. Gaviria, J. Van Caneghem, C. Vandecasteele, Improved selection of the functional unit in environmental impact assessment of cement, J. Clean. Prod. 168 (2017) 463–473, https://doi.org/10.1016/j.jclepro.2017.09.007.

[68] A. Tahsin, S. Siddique, W. Ashraf, M. Sattler, Assessment of the durability and environmental impact of seawater-activated portlandite-calcined clay binder, J. Sustain Cem. Based Mater. (2023), https://doi.org/10.1080/21650373.2023.2243480.